Supporting Information

Sarangapani et al. 10.1073/pnas.1220700110

SI Materials and Methods

Isolation of Kinetochore Particles. Kinetochore particles were isolated by affinity-purifying Dsn1-His-Flag protein using a previously-described minichromosome purification protocol (1) but with some modifications. The Ndc80-7A, Ndc80-7D, and Ndc80-WT kinetochore particles were purified from asynchronously growing cells. The Dam1 phosphomutants and all of the Ndc80 + Dam1 double mutants were purified from cells arrested in media containing benomyl to ensure that they were in the same cell-cycle stage. For benomyl arrest, YPD media containing 120 μg/mL benomyl was prepared by adding benomyl (30 mg/mL stock solution dissolved in DMSO) to boiling media and cooled to room temperature. Equivalent amounts of benomyl media were added to growing cell cultures (at OD_{600} ~0.7) so that the final benomyl concentration was 60 μg/mL. Cells were grown for an additional 3 h and harvested when greater than 90% of cells were large-budded. For both asynchronously growing and benomyl-arrested cultures, 1–5 L of cells were harvested and extract was prepared by breaking cells in a blender with dry ice, followed by ultracentrifugation. Beads conjugated with anti-Flag antibodies were incubated with extract for 3 h with constant rotation, followed by four washes with BH/0.15 [25 mM Hepes pH 8.0, 2 mM $MgCl_2$, 0.1 mM EDTA pH 8.0, 0.5 mM EGTA pH 8.0, 0.1% Nonidet P-40, 150 mM KCl, 15% (vol/vol) glycerol] containing protease inhibitors, phosphatase inhibitors, and 2 mM DTT. Beads were further washed twice with BH/0.15 with protease inhibitors. Associated proteins were eluted from the beads by gentle agitation of beads in elution buffer (0.5 mg/mL 3FLAG peptide in BH/0.15 with protease inhibitors) for 25 min at room temperature. Typical concentrations of Dsn1-His-Flag ranged between 1.5 and 4.5 μg/mL (20–60 nM Dsn1) as determined by comparing the purified material with BSA standards on silver-stained SDS/PAGE gels. Aliquots were made and stored at −80 °C.

Laser-Trap Instrument. The instrument has been described previously (2). Position sensor response was mapped using the piezo stage to raster-scan a stuck bead through the beam, and trap stiffness was calibrated along the two principle axes using the drag force, equipartition, and power spectrum methods. Force feedback was implemented with custom LabView software. During force measurements, bead-trap separation was sampled at 40 kHz; stage position was updated at 50 Hz to maintain the desired tension (force-clamp assay) or ramp-rate (force-ramp assay). Bead and stage position data were decimated to 0.2 kHz before storing to disk.

Rupture Force Measurements. Native kinetochore particles were linked to beads as previously described (3). Streptavidin-coated polystyrene beads (0.44 μm in diameter; Spherotech) were functionalized with biotinylated anti-His_5 antibodies (Qiagen) and stored with continuous rotation at 4 °C in BRB80 (80 mM Pipes, 1 mM $MgCl_2$, and 1 mM EGTA, pH 6.9) supplemented with 8 $mg{\cdot}mL^{-1}$ BSA for up to 3 mo. Immediately before each experiment, beads were decorated with kinetochore particles by incubating 6 pM anti-His_5 beads for 60 min at 4 °C with different amounts of the purified kinetochore material, corresponding to Dsn1-His-Flag concentrations ranging from 0.6 to 70 nM. Flow chambers (~10-μL volume) were constructed and functionalized as previously described (2). First, 10 μL of 10 $mg{\cdot}mL^{-1}$ biotinylated BSA (Vector Laboratories) was introduced and allowed to bind to the glass surface for 15 min at room temperature. The chamber was then washed with 100 μL of BRB80. Next, 75–100 μL of 0.33 $mg{\cdot}mL^{-1}$ avidin DN (Vector Laboratories) was introduced, incubated for 3 min, and washed out with 100 μL of BRB80. GMPCPP-stabilized biotinylated microtubule seeds were introduced in BRB80, and allowed to bind to the functionalized glass surface for 3 min. The chamber was then washed with 100 μL of growth buffer (BRB80 containing 1 mM GTP and 1 $mg{\cdot}mL^{-1}$ κ-casein). Finally, kinetochore particle-coated beads were introduced at an eightfold dilution from the incubation mix (see above) in a solution of growth buffer containing 1.5 $mg{\cdot}mL^{-1}$ purified bovine brain tubulin, 1 mM DTT, 500 $\mu g{\cdot}mL^{-1}$ glucose oxidase, 60 $\mu g{\cdot}mL^{-1}$ catalase, and 25 mM glucose. The edges of the flow chamber were sealed with nail polish to prevent evaporation. All laser-trap experiments were performed at 23 °C.

Using the laser trap, individual beads were attached to the ends of growing microtubules and preloaded with a constant force ranging between 2 and 4 pN. After a brief preload period, during which we verified that the beads were moving at a rate consistent with that of microtubule growth, the laser trap was programmed to ramp the force at a constant rate (0.25 $pN{\cdot}s^{-1}$) until the linkage ruptured, or until the load limit of the trap (~20 pN) was reached and the bead escaped from the trap. At all Dsn1-His-Flag concentrations below 60 nM, the fraction of beads that reached the load limit and escaped the trap was small (10–15%). Because only 1–2 min was required to record each individual rupture event, large populations could be measured relatively efficiently, facilitating statistical analysis. Statistics for this dataset are given in Table S1.

Force-Clamp Assay. Kinetochore-decorated beads were prepared as described above using a Dsn1:bead ratio of 200:1 (~2 nM Dsn1-His-Flag; 5.6-pM beads), which is well below the single particle limit (3). The beads were introduced into a flow cell, attached to the ends of growing microtubules, and subjected to tensile force as described above, except that the laser trap was programmed to maintain a constant mean force, ~2.5 pN. Statistics for this dataset are shown in Tables S2–S5. Attachment lifetimes were computed from the instant an attachment was fully loaded until the event ended, often because of bead detachment but sometimes for other reasons (e.g., when another bead fell into the trap). All individual event durations were considered, irrespective of how the events ended. Lifetimes (Fig. 3*D*) were computed by summing the total time of all events and dividing by the number of detachments. The rate of detachment during growth (Fig. 3*E*) and the catastrophe rate (Fig. 3*G*) were computed by counting the numbers of these events and dividing by the total microtubule assembly (growth) time. Similarly, the rates of detachment during shortening (Fig. 3*F*) and the rescue rate (Fig. 3*H*) were computed by counting events and dividing by the total microtubule disassembly (shortening) time.

Statistical Analyses. The *P* values for comparison of mean rupture forces (Fig. 2*F*, and Figs. S2*A* and S3) were computed by single-factor ANOVA. For the data in Fig. 3, we computed the *P* values from their corresponding *z*-scores, given by $z = (\mu_1 - \mu_2).(\delta_1^2 + \delta_2^2)^{-0.5}$. Here, μ_1 and μ_2 are the means of any given parameter (e.g., lifetime, catastrophe rate, and so forth) for the two molecular systems being compared (e.g., Ndc80-*7A*, or Dam1-*4D*) and δ_1 and δ_2 are the corresponding errors based on counting statistics, as detailed in Tables S2–S5. The *z*-score denotes how many SDs separate the two mean values and allows the statistical significance (or lack thereof) of their separation to be estimated.

Contributions of the Ndc80 Subcomplex to Both Initial Binding and Tip-Coupling. Across eukaryotes, kinetochore-microtubule coupling depends on the Ndc80 subcomplex, but its exact role in yeast remains a subject of discussion. Studies in metazoans suggest that kinetochore-anchored Ndc80 subcomplexes provide direct microtubule interactions that represent the primary microtubule attachment interface (4, 5). Consistent with this view, truncation of the N-terminal Ndc80 tail, which dramatically reduces its microtubule binding affinity in vitro (6–9), also severely destabilizes kinetochore-microtubule attachments in metazoan cells (10–13). However, yeast survive truncation of the Ndc80 tail (14, 15), and it has been suggested that Ndc80 in yeast may instead act mainly as a scaffold onto which other microtubule-binding subcomplexes, such as Dam1, must assemble to form the primary interface (16). In our view, the idea that yeast Ndc80 acts solely as a scaffold is difficult to reconcile with the available data. Yeast kinetochores make initial, Ndc80-dependent lateral attachments to microtubules even when the Dam1 complex is disrupted, both in vivo (17) and also in vitro (Fig. S2*B*) (3). Phosphomimetic mutations on Ndc80 also weaken the tip-coupling strength of yeast kinetochore particles by an equivalent amount, regardless of the state of the Dam1 complex (Fig. 3*F* and Fig. S2*A*). Thus, Ndc80 makes contributions to initial attachment, and also to tip-coupling strength, that appear to be independent of Dam1. Moreover, tail truncation does not completely abolish the affinity of Ndc80 for microtubules (6–9, 18). Thus, the viability of yeast lacking the tail of Ndc80 probably reflects a difference in the degree to which they rely on the tail, or a functional redundancy between the Ndc80 and Dam1 complexes (14, 18), rather than a fundamental difference in the role of Ndc80.

1. Akiyoshi B, Nelson CR, Ranish JA, Biggins S (2009) Quantitative proteomic analysis of purified yeast kinetochores identifies a PP1 regulatory subunit. *Genes Dev* 23(24): 2887–2899.
2. Franck AD, Powers AF, Gestaut DR, Davis TN, Asbury CL (2010) Direct physical study of kinetochore-microtubule interactions by reconstitution and interrogation with an optical force clamp. *Methods* 51(2):242–250.
3. Akiyoshi B, et al. (2010) Tension directly stabilizes reconstituted kinetochore-microtubule attachments. *Nature* 468(7323):576–579.
4. Cheeseman IM, Desai A (2008) Molecular architecture of the kinetochore-microtubule interface. *Nat Rev Mol Cell Biol* 9(1):33–46.
5. DeLuca JG, Musacchio A (2012) Structural organization of the kinetochore-microtubule interface. *Curr Opin Cell Biol* 24(1):48–56.
6. Alushin GM, et al. (2012) Multimodal microtubule binding by the Ndc80 kinetochore complex. *Nat Struct Mol Biol* 19(11):1161–1167.
7. Ciferri C, et al. (2008) Implications for kinetochore-microtubule attachment from the structure of an engineered Ndc80 complex. *Cell* 133(3):427–439.
8. Umbreit NT, et al. (2012) The Ndc80 kinetochore complex directly modulates microtubule dynamics. *Proc Natl Acad Sci USA* 109(40):16113–16118.
9. Wei RR, Al-Bassam J, Harrison SC (2007) The Ndc80/HEC1 complex is a contact point for kinetochore-microtubule attachment. *Nat Struct Mol Biol* 14(1):54–59.
10. DeLuca JG, et al. (2005) Hec1 and nuf2 are core components of the kinetochore outer plate essential for organizing microtubule attachment sites. *Mol Biol Cell* 16(2): 519–531.
11. DeLuca JG, Moree B, Hickey JM, Kilmartin JV, Salmon ED (2002) hNuf2 inhibition blocks stable kinetochore-microtubule attachment and induces mitotic cell death in HeLa cells. *J Cell Biol* 159(4):549–555.
12. Guimaraes GJ, Dong Y, McEwen BF, Deluca JG (2008) Kinetochore-microtubule attachment relies on the disordered N-terminal tail domain of Hec1. *Curr Biol* 18(22): 1778–1784.
13. McCleland ML, et al. (2003) The highly conserved Ndc80 complex is required for kinetochore assembly, chromosome congression, and spindle checkpoint activity. *Genes Dev* 17(1):101–114.
14. Demirel PB, Keyes BE, Chaterjee M, Remington CE, Burke DJ (2012) A redundant function for the N-terminal tail of Ndc80 in kinetochore-microtubule interaction in *Saccharomyces cerevisiae*. *Genetics* 192(2):753–756.
15. Kemmler S, et al. (2009) Mimicking Ndc80 phosphorylation triggers spindle assembly checkpoint signalling. *EMBO J* 28(8):1099–1110.
16. Lampert F, Hornung P, Westermann S (2010) The Dam1 complex confers microtubule plus end-tracking activity to the Ndc80 kinetochore complex. *J Cell Biol* 189(4): 641–649.
17. Tanaka K, et al. (2005) Molecular mechanisms of kinetochore capture by spindle microtubules. *Nature* 434(7036):987–994.
18. Lampert F, Mieck C, Alushin GM, Nogales E, Westermann S (2013) Molecular requirements for the formation of a kinetochore-microtubule interface by Dam1 and Ndc80 complexes. *J Cell Biol* 200:21–30.

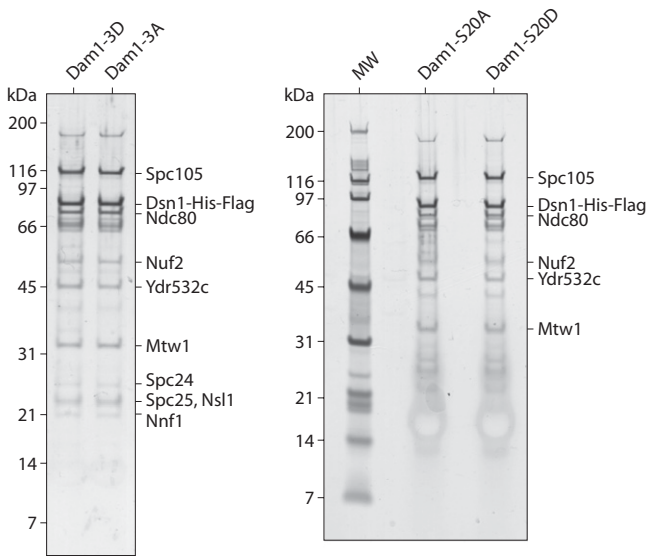

Fig. S1. Purification of additional phospho-mutant kinetochore particles. The relative abundance of core kinetochore proteins that copurified with Dsn1-His-Flag was similar for Dam1-3D (SBY10342), Dam1-3A (SBY10457), Dam1-S20A (SBY10278), and Dam1-S20D (SBY10280). Proteins were separated by SDS/PAGE and detected by silver staining, as in Fig. 1*B*.

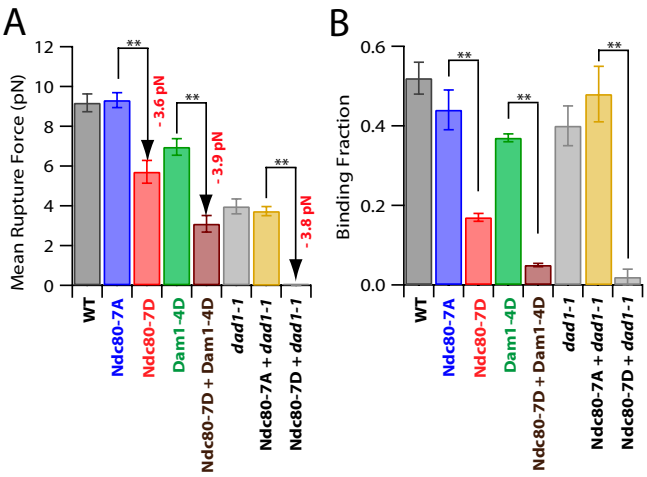

Fig. S2. The Ndc80 and Dam1 subcomplexes play distinct roles in kinetochore particle behavior. (*A*) The reduction in rupture strength caused by phosphomimetic substitutions on the Ndc80 subcomplex is independent of the status of the Dam1 subcomplex. All data from Fig. 2*F* are replotted here, together with mean rupture forces measured for the double-mutants, Ndc80-7A + *dad1-1* (SBY9469) and Ndc80-7D + *dad1-1* (SBY9470). In three different contexts, the reduction in strength because of Ndc80-7D (indicated by arrows) was roughly equivalent. Error bars represent SEM (n = 6–80 events, as indicated in Table S1). (*B*) Initial binding depends mainly on the Ndc80 subcomplex, with little dependence on the Dam1 subcomplex. Bars represent the fraction of beads, prepared at ~6 nM Dsn1 (corresponding to the gray shaded regions in Fig. 2 *C* and *D*), that bound a growing microtubule. Phosphomimetic substitutions on the Ndc80 subcomplex strongly reduced binding, whereas mutating the Dam1 subcomplex did not. Error bars represent SD (n = 2–20 experiments, as indicated in Table S1). $^{**}P < 0.05$ (statistically significant differences). Data for wild-type (WT, SBY8253) and *dad1-1* alone (SBY8460) in *A* and *B* are from ref. 3.

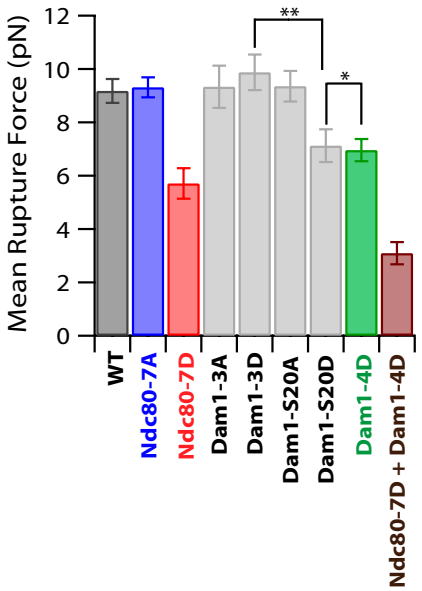

Fig. S3. Serine 20 of the Dam1 protein is a key phospho-regulatory site. All data from Fig. 2*F* are replotted here, together with mean rupture forces measured for the additional phospho-mutants, Dam1-3A (SBY10457), Dam1-3D (SBY10342), Dam1-S20A (SBY10278), and Dam1-S20D (SBY10280). The strength of the one-site phosphomimetic, Dam1-S20D (SBY10280), is indistinguishable from that of the four-site phosphomimetic, Dam1-4D (SBY9021). The strength of the three-site phosphomimetic, Dam1-3D (SBY10342), is indistinguishable from wild-type (SBY8253, from ref. 3) and from the phospho-deficient controls, Ndc80-7A (SBY8522), Dam1-3A (SBY10457), and Dam1-S20A (SBY10278). Error bars represent SD (n = 2–20 experiments, as indicated in Table S1). **$P < 0.05$ (statistically significant difference). *$P > 0.1$ (lack of significance).

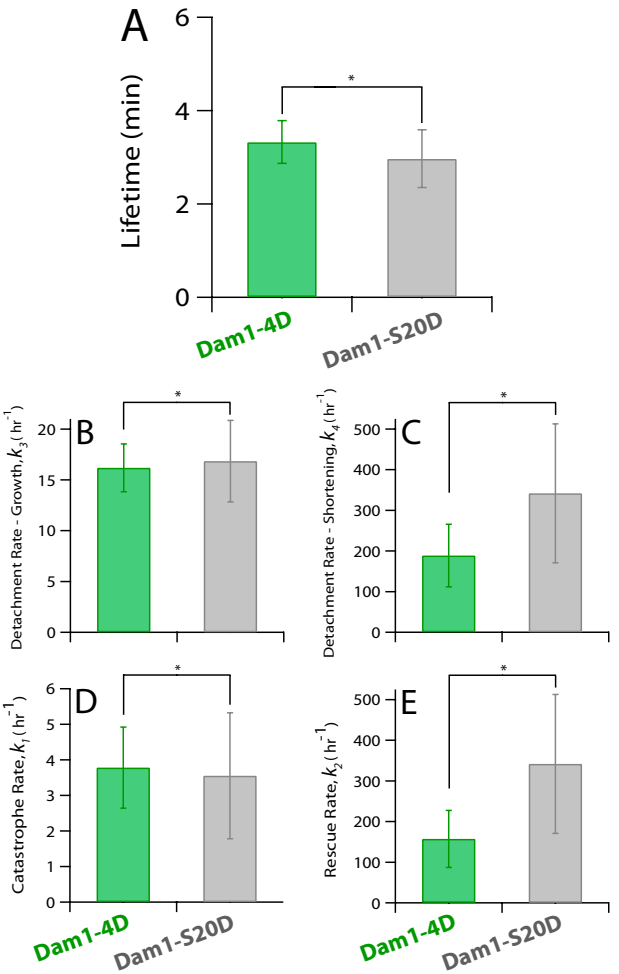

Fig. S4. Additional evidence that serine 20 of the Dam1 protein is a key phospho-regulatory site. Data from the force-clamp experiments of Figs. 3 *D–H* for the four-site phosphomimetic Dam1-4D are replotted here (green bars), together with the attachment lifetime (*A*), detachment rate during growth (*B*), detachment rate during shortening (*C*), catastrophe rate (*D*), and rescue rate (*E*) for the one-site phosphomimetic, Dam1-S20D (gray bars, SBY10280). The force-clamp behavior of Dam1-S20D is indistinguishable from that of Dam1-4D (SBY9021), as we also found in force-ramp experiments (Fig. S3). Error bars represent uncertainty due to counting statistics. *$P > 0.1$ (lack of statistical significance).

Table S1. Statistics for rupture force experiments

Kinetochore	~1nM (0.6–2 nM) Dsn1		~2 nM (1–4 nM) Dsn1		~6 nM (6–8 nM) Dsn1		~65 nM (60–70 nM) Dsn1	
	Binding fraction	Rupture force (pN)	Binding fraction	Rupture force (pN)	Binding fraction	Rupture force (pN)	Binding fraction	Rupture force (pN)
Wild-type*	0.07 ± 0.02 (n = 6)	9.29 ± 0.58 (n = 43)	0.13 ± 0.02 (n = 7)	8.90 ± 0.51 (n = 64)	0.52 ± 0.04 (n = 7)	9.18 ± 0.45 (n = 70)	0.94 ± 0.09 (n = 4)	8.97 ± 0.59 (n = 47)
Ndc80-WT†					0.41 ± 0.07 (n = 2)	8.32 ± 0.48 (n = 50)		
Ndc80-7A	0.07 ± 0.01 (n = 4)	8.99 ± 0.42 (n = 62)	0.10 ± 0.01 (n = 12)	8.98 ± 0.42 (n = 55)	0.44 ± 0.05 (n = 3)	9.31 ± 0.38 (n = 80)	0.87 ± 0.01 (n = 2)	9.85 ± 1.08 (n = 6)
Ndc80-7D	0.045 ± 0.004 (n = 2)	5.73 ± 0.44 (n = 42)	0.10 ± 0.02 (n = 20)	5.84 ± 0.51 (n = 42)	0.17 ± 0.01 (n = 3)	5.71 ± 0.57 (n = 52)	0.50 ± 0.01 (n = 2)	7.01 ± 0.74 (n = 34)
Dam1-4A	No data available because these cells are inviable‡							
Dam1-4D			0.10 ± 0.01 (n = 9)	6.82 ± 0.59 (n = 36)	0.37 ± 0.01 (n = 2)	6.96 ± 0.42 (n = 42)		
Ndc80-7D + Dam1-4D					0.05 ± 0.004 (n = 2)	3.09 ± 0.42 (n = 13)		
Dam1-3A					0.47 ± 0.04 (n = 2)	9.33 ± 0.79 (n = 29)		
Dam1-3D					0.55 ± 0.05 (n = 2)	9.87 ± 0.67 (n = 26)		
Dam1-S20A					0.48 ± 0.03 (n = 3)	9.35 ± 0.57 (n = 45)		
Dam1-S20D			0.10 ± 0.01 (n = 4)		0.48 ± 0.08 (n = 2)	7.12 ± 0.61 (n = 31)		
*dad1-1**					0.40 ± 0.05 (n = 6)	3.97 ± 0.37 (n = 60)		
Ndc80-7A + *dad1-1*					0.48 ± 0.07 (n = 3)	3.75 ± 0.23 (n = 57)		
Ndc80-7D + *dad1-1*					0.02 ± 0.02 (n = 2)	–0-		

Binding fractions indicate the proportion of beads that bound when held near the tip of a growing microtubule, expressed as mean ± SD from n experiments. The number of individual beads tested during each experiment ranged from 5 to 50. Rupture forces indicate mean ± SEM from n individual rupture events. The Dsn1 concentrations used for bead decoration were slightly different for the various mutants, and are grouped here into four categories with mean values (~) and ranges indicated. The colors for kinetochore types Ndc80-7A (blue), Ndc80-7D (red), Dam1-4D (green), and Ndc80-7D + Dam1-4D (brown) were chosen to match those in Figs. 2 and 3, and Figs. S2–S4.

*Published previously in Akiyoshi et al. (1).

†Wild-type Ndc80 integrated at a different locus (SBY8524), as a control for Ndc80-7A and Ndc80-7D mutants.

‡Ref. 2.

1. Akiyoshi B, et al. (2010) Tension directly stabilizes reconstituted kinetochore-microtubule attachments. *Nature* 468(7323):576–579.
2. Cheeseman IM, et al. (2002) Phospho-regulation of kinetochore-microtubule attachments by the Aurora kinase Ipl1p. *Cell* 111(2):163–172.

Table S2. Statistics for force-clamp (constant force) experiments: Total lifetimes

Kinetochore	Mean clamp force ± error (pN)	Total no. detachments	Lifetime ± error (min)
Ndc80-7A	2.57 ± 0.62	16	26.28 ± 6.57
Ndc80-7D	2.58 ± 0.55	22	13.31 ± 2.83
Dam1-4D	2.36 ± 1.41	53	3.33 ± 0.46
Dam1-S20D	1.88 ± 1.48	23	2.97 ± 0.62

To calculate mean attachment lifetimes, the total time (spent in growth and shortening) was divided by the total number of detachments (from growing or shortening microtubules). Estimated errors represent uncertainty because of counting statistics, which were computed as $\delta = \mu \cdot N^{-1}\sqrt{N}$, where μ is the mean rate (or lifetime) and $N^{-1}\sqrt{N}$ is the fractional uncertainty. The colors for kinetochore types Ndc80-7A (blue), Ndc80-7D (red), and Dam1-4D (green) were chosen to match those in Figs. 2 and 3 and Figs. S2–S4.

Table S3. Statistics for force-clamp (constant force) experiments: Growing tips

Kinetochore	Mean clamp force ± error (pN)	No. detachments (growing tips)	Total growth time (h)	Detachment rate, growth ± error (h^{-1})	No. catastrophes	Catastrophe rate ± error (h^{-1})
Ndc80-7A	2.57 ± 0.62	9	6.95	1.30 ± 0.43	10	1.44 ± 0.46
Ndc80-7D	2.58 ± 0.55	17	4.86	3.50 ± 0.85	6	1.23 ± 0.50
Dam1-4D	2.36 ± 1.41	47	2.91	16.18 ± 2.36	11	3.78 ± 1.14
Dam1-S20D	1.88 ± 1.48	19	1.13	16.85 ± 3.87	4	3.55 ± 1.77

Mean rates for detachment from growing microtubules and for catastrophe were calculated by dividing the number of events by the total observed growth time. Estimated errors represent uncertainty because of counting statistics, which were computed as $\delta = \mu \cdot N^{-1}\sqrt{N}$, where μ is the mean rate (or lifetime) and $N^{-1}\sqrt{N}$ is the fractional uncertainty. The colors for kinetochore types Ndc80-7A (blue), Ndc80-7D (red), and Dam1-4D (green) were chosen to match those in Figs. 2 and 3 and Figs. S2–S4.

Table S4. Statistics for force-clamp (constant force) experiments: Shortening tips

Kinetochore	Mean clamp force ± error (pN)	No. detachments (shortening tips)	Total shortening time (h)	Detachment rate, shortening ± error (h^{-1})	No. rescues	Rescue rate ± error (h^{-1})
Ndc80-7A	2.57 ± 0.62	7	0.060	117.62 ± 44.46	10	168.03 ± 53.14
Ndc80-7D	2.58 ± 0.55	5	0.016	320.34 ± 143.26	3	192.21 ± 110.97
Dam1-4D	2.36 ± 1.41	6	0.032	188.55 ± 76.97	5	157.12 ± 70.27
Dam1-S20D	1.88 ± 1.48	4	0.012	341.76 ± 170.88	4	341.76 ± 170.88

Mean rates for detachment from shortening microtubules and for rescue were calculated by dividing the number of events by the total observed shortening time. Estimated errors represent uncertainty because of counting statistics, which were computed as $\delta = \mu \cdot N^{-1}\sqrt{N}$, where μ is the mean rate (or lifetime) and $N^{-1}\sqrt{N}$ is the fractional uncertainty. The colors for kinetochore types Ndc80-7A (blue), Ndc80-7D (red), and Dam1-4D (green) were chosen to match those in Figs. 2 and 3 and Figs. S2–S4.

Table S5. Statistics for force-clamp (constant force) experiments: P values

	P value				
Kinetochores compared	Lifetime	Detachment rate, growth	Detachment rate, shortening	Catastrophe rate	Rescue rate
Ndc80-7A vs. Ndc80-7D	**0.02****	**0.04****	0.12*	0.39*	0.19*
Ndc80-7A vs. Dam1-4D	**0.0001****	**0****	0.21*	**0.03****	0.33*
Dam1-4D vs. Dam1-S20D	0.68*	0.54*	0.16*	0.44*	0.79*

The colors for kinetochore types Ndc80-7A (blue), Ndc80-7D (red), and Dam1-4D (green) were chosen to match those in Figs. 2 and 3 and Figs. S2–S4. Statistically significant differences are shown in boldface. *P* values were calculated from *z*-scores, as detailed in *SI Materials and Methods*. $^{**}P < 0.05$; $^{*}P > 0.1$.

Table S6. Yeast strains used in this study

Strain	Genotype
SBY8253	*MATa ura3-1 leu2,3-112 his3-11 trp1-1 ade2-1 LYS2 can1-100 bar1-1 DSN1-6HIS-3FLAG::URA3*
SBY8460	*MATa ura3-1 leu2,3-112 his3-11 trp1-1::256lacO::TRP1 ade2-1 can1-100 LYS2 bar1-1 DSN1-6HIS-3FLAG:URA3 dad1-1::KAN*
SBY8522	*MATa ura3-1 leu2,3-112 his3-11 trp1-1 ade2-1 LYS2 can1-100 bar1-1 DSN1-6HIS-3FLAG::URA3 ndc80::NAT::ndc80(T21A,S37A,T54A, T71A,T74A,S95A, S100A)::TRP1*
SBY8523	*MATa ura3-1 leu2,3-112 his3-11 trp1-1 ade2-1 LYS2 can1-100 bar1-1 DSN1-6HIS-3FLAG::URA3 ndc80::NAT::ndc80(T21E,S37D,T54E, T71E,T74E,S95D, S100E)::TRP1*
SBY8524	*MATa ura3-1 leu2,3-112 his3-11 trp1-1 ade2-1 LYS2 can1-100 bar1-1 DSN1-6HIS-3FLAG::URA3 ndc80::NAT::NDC80::TRP1*
SBY9020	*MATa ura3-1 leu2,3-112 his3-11 trp1-1 ade2-1 lys2Δ can1-100 bar1-1 DSN1-6HIS-3FLAG::URA3 ndc80::NAT::ndc80(T21E,S37D,T54E, T71E,T74E,S95D, S100E)::TRP1 dam1(S20D,S257D,S265D,S292D)::KanMX*
SBY9021	*MATa ura3-1 leu2,3-112 his3-11 trp1-1 ade2-1 lys2Δ can1-100 bar1-1 DSN1-6HIS-3FLAG::URA3 dam1(S20D,S257D,S265D,S292D):: KanMX*
SBY9469	*MATa ura3-1 leu2,3-112 his3-11 trp1-1::256lacO::TRP1 ade2-1 LYS2 can1-100 bar1-1 DSN1-6HIS-3FLAG::URA3 dad1-1::KanMX ndc80::NAT::ndc80(T21A, S37A,T54A,T71A,T74A,S95A,S100A)::TRP1*
SBY9470	*MATa ura3-1 leu2,3-112 his3-11 trp1-1::256lacO::TRP1 ade2-1 LYS2 can1-100 bar1-1 DSN1-6HIS-3FLAG::URA3 dad1-1::KanMX ndc80::NAT::ndc80(T21E, S37D,T54E,T71E,T74E,S95D,S100E)::TRP1*
SBY9471	*MATa ura3-1 leu2,3-112 his3-11 trp1-1::256lacO::TRP1 ade2-1 LYS2 can1-100 bar1-1 DSN1-6HIS-3FLAG::URA3 dad1-1::KanMX ndc80::NAT::NDC80::TRP1*
SBY10278	*MATa ura3-1 leu2,3-112 his3-11 trp1-1 ade2-1 LYS2 can1-100 bar1-1 DSN1-6HIS-3FLAG::URA3 dam1(S20A)::KanMX*
SBY10280	*MATa ura3-1 leu2,3-112 his3-11 trp1-1 ade2-1 LYS2 can1-100 bar1-1 DSN1-6HIS-3FLAG::URA3 dam1(S20D)::KanMX*
SBY10342	*MATa ura3-1 leu2,3-112 his3-11 trp1-1 ade2-1 LYS2 can1-100 bar1-1 DSN1-6HIS-3FLAG::URA3 dam1(S257D, S265D, S292D)::KanMX*
SBY10457	*MATa ura3-1 leu2,3-112 his3-11 trp1-1 ade2-1 LYS2 can1-100 bar1-1 DSN1-6HIS-3FLAG::URA3 dam1(S257A, S265A, S292A)::KanMX*

All strains are isogenic with the W303 background. The *Ndc80-7D* (*T21E,S37D,T54E,T71E,T74E,S95D,S100E*) strain was made as described in ref. 1 and shows no obvious growth defect in vivo.

1. Akiyoshi B, Nelson CR, Ranish JA, Biggins S (2009) Analysis of Ipl1-mediated phosphorylation of the Ndc80 kinetochore protein in *Saccharomyces cerevisiae*. *Genetics* 183(4):1591–1595.